Sustainable Energy & Fuels

COMMUNICATION

Cite this: *Sustainable Energy Fuels*, 2019, **3**, 1966

Received 9th May 2019
Accepted 13th June 2019

DOI: 10.1039/c9se00291j

rsc.li/sustainable-energy

Effect of soluble sulfur species on the electrochemical behavior of lithium–sulfur batteries with dual-phase electrolytes†

Chengcheng Zhao, Hao Yang, Xiaofei Wang, Huilan Li, Chu Qi, Lina Wang* and Tianxi Liu

Lithium polysulfides (Li_2S_n, $2 < n \leq 8$) are investigated as a catholyte for lithium–sulfur (Li–S) batteries with dual-phase electrolytes. The combined electrochemical and morphological investigation reveals that the cell with Li_2S_n shows higher electrochemical activity and faster reaction kinetics compared to that with S_8, providing an attractive alternative for high energy density rechargeable flow batteries.

Lithium–sulfur (Li–S) batteries are a promising power supply candidate for electric vehicles and grid storage systems. The reaction between elemental sulfur (S_8) and metallic lithium involves the exchange of 2 electrons per mole of sulfur ($S_8 + 16Li \leftrightarrow 8Li_2S$), which allows for a high theoretical capacity of 1672 mA h g^{-1} and a large theoretical gravimetric energy density of 2600 Wh Kg^{-1}.[1] In spite of their considerable advantages, broad adaption of Li–S batteries has been hampered by their fast self-discharge, low energy efficiency and poor cycling stability. Problems originate from sulfur chemistry related to the intrinsic electrical insulating features of S_8 (5×10^{-30} S cm^{-1}) and the end discharge product Li_2S (10^{-13} S cm^{-1}), the large volumetric change between them and the shuttle effect of electrolyte-soluble intermediates of polysulfides (Li_2S_n, $2 < n \leq 8$).[2] During cycling, polysulfides may diffuse throughout the cells, triggering parasitic reactions with metallic Li and consequently leading to active material loss, serious corrosion reactions on the Li-anode surface and inhomogeneous aggregation of S_8/Li_2S. From another point of view, the robust reactions between polysulfides and Li result in the *in situ* generation of Li_2S/Li_2S_2, which can passivate and stabilize the anode surface. However, the surface deposition is insulating and unstable during repeated charge–discharge processes, resulting in undesirable capacity fading.

Besides the extensive efforts that have been devoted to the impregnation of sulfur into various functionalized sulfur cathodes,[3] designing alternative electrolytes to minimize Li_2S_n solubility is another approach to address these obstacles.[4] As a matter of fact, once a liquid organic electrolyte is used, diffusion of continuously generated soluble polysulfide species is thermodynamically inevitable. Moreover, because of the intrinsic insulation of solid S_8 and Li_2S, the solubility and reactivity of these Li_2S_n species are important contributors to the overall electrochemical reactions. Suppression of their solubility comes at the cost of decreased energy efficiency and power density.[4b,5] Hence, the game-changing shift from a one-phase to a dual-phase electrolyte has provided a facile strategy to eliminate the aforementioned polysulfide shuttle process.[6] In this case, the catholyte containing soluble sulfur species is separated from the Li anode by a Li^+ selective separator, which is permeable to Li^+ while being impermeable to S_n^{2-}. The adverse effects associated with Li_2S_n shuttling are thus avoided. And the cell architecture permits a flexible extension to a flow-through mode, guaranteeing a promising model for future grid-scale energy storage.

However, the low solubility of S_8 in a vast majority of solvents strongly increases the system storage size and limits its practical application in flow batteries. For instance, the maximum solubility of S_8 in tetrahydrofuran (THF) is ~0.3 M (on the basis of S) at room temperature.[7] To achieve a higher volumetric energy density, electrolytes with highly concentrated sulfur species are need. From this perspective, Li_2S_n is more promising given that the saturated concentration of S (in the form of Li_2S_n) in organic solutions is as high as 10 M.[7a] In this work, the Li_2S_n catholyte prepared *via* simple chemical reaction of Li_2S with Li or S_8 is introduced for Li–S batteries with dual-phase electrolytes. The reaction kinetics of the cell with Li_2S_n is investigated in comparison with that using S_8. Besides the contribution to reversible capacity as electroactive species, Li_2S_n is also demonstrated to facilitate ion transport as a supporting electrolyte salt and a chemical reaction mediator, offering new opportunities for designing next-generation flow batteries.

State Key Laboratory for Modification of Chemical Fibers and Polymer Materials, College of Materials Science and Engineering, Innovation Center for Textile Science and Technology, Donghua University, Shanghai 201620, China. E-mail: linawang@dhu.edu.cn

† Electronic supplementary information (ESI) available. See DOI: 10.1039/c9se00291j

The architecture of the proposed Li–S cell with a dual-phase electrolyte is illustrated in Fig. 1, in which the Li_2S_n-based catholyte and the anolyte for the Li anode are separated by a Li^+-ion conductive $Li_{1+x+y}Al_xTi_{2-x}Si_yP_{3-y}O_{12}$ (LATP) membrane. THF solution containing soluble Li_2S_n and 1 M $LiClO_4$ is employed as the catholyte. Here, $LiClO_4$ is the basic catholyte salt for sufficient ionic conductivity during the whole electrochemical process. Li_2S_n acts as an electrochemical active material as well as a supporting salt in the catholyte. The Li anode is immersed in the anolyte of ethylene carbonate/dimethyl carbonate (EC/DMC, 3/7, v/v) with 1 M $LiPF_6$. If not specially mentioned, Li_2S_n is prepared from the reaction of 0.2 M S with excess metallic Li ($2Li + n/8S_8 \rightarrow Li_2S_n$) in THF, giving rise to a dark brown solution (inset in Fig. 2a). Elemental analysis (Table S1, ESI†) indicates that the overall composition of Li_2S_n is $Li_2S_{2.51}$, implying that Li_2S_n species with a distribution of n values above 2 are present in solution. Here, a "mixture" of lithium polysulfide species with different chain lengths rather than the nominal Li_2S_n composition is obtained because of the disproportionation reaction.[8] UV-visible absorption analysis of the catholyte was conducted with pure THF solvent as a blank and THF solution containing $LiClO_4$ as a reference sample (Fig. S1, ESI†). Deconvolution of the spectrum yields two sharp peaks at 225 nm and 275 nm.[8,9] The peak at 225 nm corresponds to ClO_4^-, while the 275 nm peak is assigned to S_3^{2-}. Several weak signals in response to higher order polysulfides such as S_4^{2-}, S_6^{2-} and S_8^{2-} are present as well. A colorless THF solution containing 0.2 M sulfur (S) and 1 M $LiClO_4$ was also prepared as a control catholyte (inset in Fig. 2b). The specific capacity values are calculated according to the mass of S.

The Li–S cell with S_8 exhibits an open-circuit voltage (OCV) above 3.0 V, while it is ~2.3 V with Li_2S_n, reflecting the different potential states of Li_2S_n and S_8. The multiple redox reaction process of cathodic active materials with Li^+ is firstly investigated by cyclic voltammetry (CV). Being distinguishable from S_8, the Li_2S_n here can be delithiated first. As presented in Fig. 2a, after a gradual current slope, an anodic current peak is present at 2.51 V. The process is regarded as the oxidation of low-order polysulfide to high-order polysulfide, and then to elemental sulfur ($S_n^{2-} \rightarrow S_8$). The CV curve displays three stepwise cathodic current peaks at voltages of 2.37, 2.10 and 1.95 V in the subsequent inverse voltage sweep from 3.0 to 1.5 V. The process is presumably relevant to the opening of ring-shaped S_8 and the breakage of linear polysulfide chains towards lower order ($S_8 \rightarrow S_n^{2-} \rightarrow Li_2S_2/Li_2S$). The cell with the S_8 catholyte has to be lithiated firstly from OCV to 1.5 V (Fig. 2b). Four apparent successive reduction steps are observed at voltages of 2.32, 2.24, 2.10 and 1.95 V, respectively, and are ascribed to the following conversions: $S_8 \rightarrow S_8^{2-} \rightarrow S_6^{2-} \rightarrow S_4^{2-} \rightarrow Li_2S_2/Li_2S$. The peak currents and positions are not completely overlapped for Li_2S_n and S_8 catholytes, which can be seen more clearly in Fig. S2 (ESI†). The first reduction peak at 2.37 V appears to be more positive for the cell with Li_2S_n than that at 2.32 V with S_8. In addition, it can be seen that the reductions from $S_8 \rightarrow S_8^{2-}$ and $S_8^{2-} \rightarrow S_6^{2-}$ have been merged together for the cell with Li_2S_n, indicating an improved reaction kinetics. In the subsequent 2nd and 3rd sweeps, the cathodic peaks at 2.10 V for Li_2S_n or S_8 shift to a lower potential with higher intensity. The anodic peak for the cell with Li_2S_n appears sharper and shifts less to a higher potential than that with S_8, indicating a faster charge transfer in the Li_2S_n-containing cell.

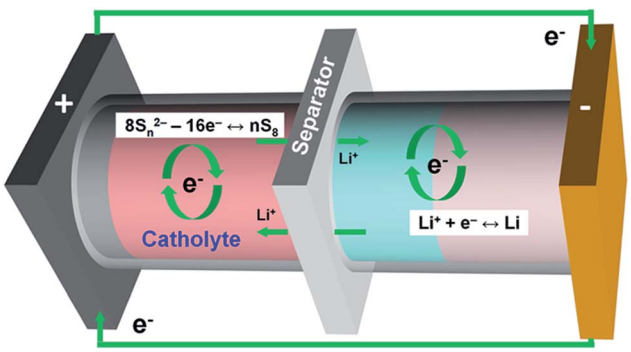

Fig. 1 Schematic architecture of a Li–S cell with a dual-phase electrolyte, in which the catholyte is the Li_2S_n-based solution.

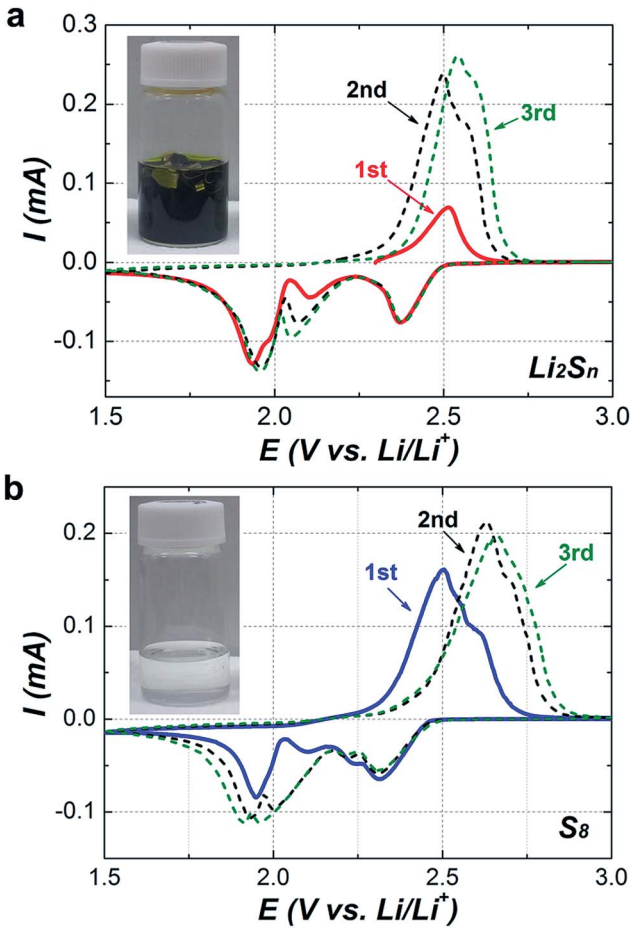

Fig. 2 Cyclic voltammogram (CV) curves for the first 3 cycles of Li–S cells with (a) Li_2S_n and (b) S_8 catholytes in the voltage range of 1.5–3 V (*vs.* Li/Li^+) at a sweeping rate of 0.01 mV s^{-1}. The inset is the digital picture of the as-prepared Li_2S_n and S_8 catholyte solutions, respectively.

Galvanostatic charge–discharge tests reveal a higher utilization of Li_2S_n than S_8. After a delithiation process on the 1st charge, the cell employing Li_2S_n exhibits similar electrochemical characteristics to S_8 (Fig. 3a and b). Both of the cells clearly show the multistage redox process, increased specific capacity upon initial cycling, stable capacity retention upon prolonged cycling and 100% coulombic efficiency (CE) at the current rate of 0.1C (1C = 1672 mA g^{-1}). The initial increased capacity suggests that the reaction kinetics is gradually accelerated through activation and stabilization of electrochemically active species. Notably, the cell with Li_2S_n displays an obviously higher specific capacity than that with S_8. As Fig. 3c shows, after the initial cycles of activation, a stabilized specific capacity approaching 1670 mA h g^{-1} is achieved and retained after 50 cycles. This means that the active material of S in the form of Li_2S_n is nearly fully utilized as a result of the improved reaction kinetics in addition to the elimination of polysulfide shuttling. In contrast, the cell with S_8 displays a capacity less than 1200 mA h g^{-1}, suggesting a relatively lower S utilization. Similarly, at an even higher current rate of 0.2C, the cell with the Li_2S_n catholyte delivers a capacity of 1135 mA h g^{-1} in the 100th cycle (Fig. S3, ESI†). A smaller capacity of 780 mA h g^{-1} is presented for the cell with S_8. To further confirm the stability of the as-designed Li–S battery, the cycled LATP and catholyte were examined. The structural change is not detectable from the X-ray diffraction (XRD) patterns of LATP before and after 100 cycles at 0.2C (Fig. S4a, ESI†). The capacity could be fully released at a low current rate of 0.025C with a newly reassembled cell by using the catholyte collected from the cycled cell with Li_2S_n (Fig. S4b, ESI†), suggesting the stability of the catholyte. The electrochemical performance strongly suggests generally improved kinetic characteristics of Li_2S_n with Li^+, which is associated with a lower interfacial charge transfer resistance. The electrochemical impedance spectra (EIS) measured at various temperatures provide further insights into the reaction kinetics. The Nyquist plots of the cell with Li_2S_n are composed of three semicircles and a short straight line (Fig. 4a). In contrast, the EIS of the cell with S_8 are composed of two semicircles in the high frequency region and a long sloping line in the low frequency region (Fig. 4b). The interfacial resistance values at high frequency, indicated by the intersection of the second semicircles with the real (Z) axis, are 2210, 1268, 828, 462 and 365 Ω at 5, 15, 25, 35 and 45 °C, respectively, and are much higher than the corresponding values of 1324, 813, 522, 320 and 307 Ω, respectively, for the cell with Li_2S_n. The long sloping line at low frequency is a part of a big semicircle, suggesting a huge charge transfer resistance. The overall charge transfer resistance of the cell with S_8 is much higher than that of the cell with Li_2S_n in the full frequency region of 1 MHz to 10 mHz.

On basis of the above results, the kinetically improved electrochemical performance of Li_2S_n can be expected to result from two aspects: (1) Li_2S_n serving as the active material as well as a supporting electrolyte salt produces a more efficient charge transfer among the interfaces of cell components. (2) The decomposition of the solid discharge product Li_2S upon charge includes both electrochemical and chemical reactions. The final discharge product Li_2S can be detected *via* nuclear magnetic resonance spectroscopy (^{1}H NMR). For the atmospheric sensitivity of polysulfide species, we adopted the organic conversion method by transferring S in the discharge product into more stable benzylized polysulfide species (Bz_2S_x, $x \geq 1$) without changing the number of S atoms.[10] Bz_2S_x can be analyzed *via* 1H NMR in the region of 3.5–4.5 ppm. A single characteristic peak assigned to Bz_2S at 3.6 ppm is present in the spectra of the carbon current collectors for the S_8 and Li_2S_n catholytes after the 1st discharge, in accordance with that of the Li_2S reference (Fig. S5a, ESI†). No peaks assigned to other polysulfides are detected, suggesting that the final solid discharge product is Li_2S. The precipitation and decomposition behavior of Li_2S from the catholyte solution was investigated by scanning electron microscopy (SEM) of the carbon current collector. SEM images reveal that the Li_2S precipitate is formed after the 1st discharge irrespective of using the Li_2S_n or S_8 catholyte (Fig. S5b and c, ESI†). However, residual Li_2S particles are clearly observed after the 1st recharge for the cell with S_8 (Fig. S5d, ESI†), which is consistent with the low initial CE of 81.7%. With regard to the cell with Li_2S_n, the Li_2S particles are almost fully decomposed after the subsequent full recharge to 3.0 V (Fig. S5e, ESI†), resulting in a high CE of 99%. The lithium

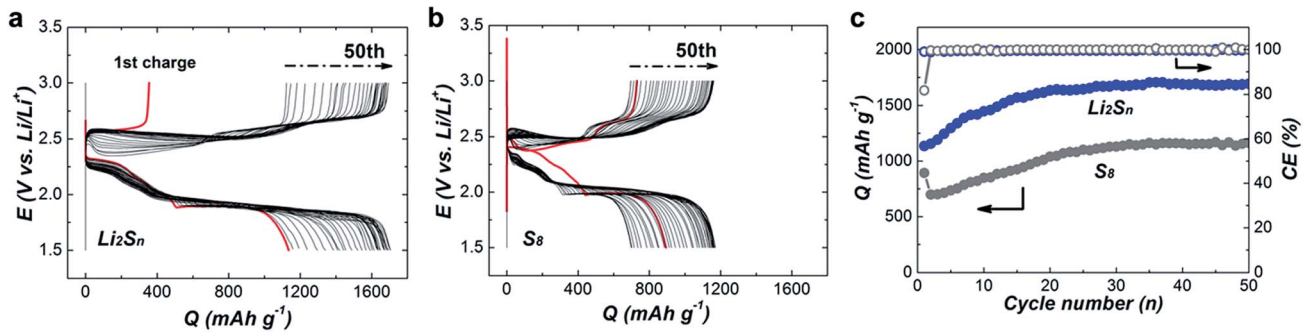

Fig. 3 Cycling performance of Li–S cells with the Li_2S_n or S_8 catholyte in the voltage range of 1.5–3 V (*vs.* Li/Li^+) at a current rate of 0.1C (1C = 1672 mA g^{-1}). (a and b) Charge–discharge curves for 50 rounds of cycling with the (a) Li_2S_n and (b) S_8 catholytes. The initial cycles are marked in red. (c) Corresponding cycling profiles with respect to specific discharge capacity and coulombic efficiency (CE). The specific capacity is calculated on the basis of the mass of sulfur (S).

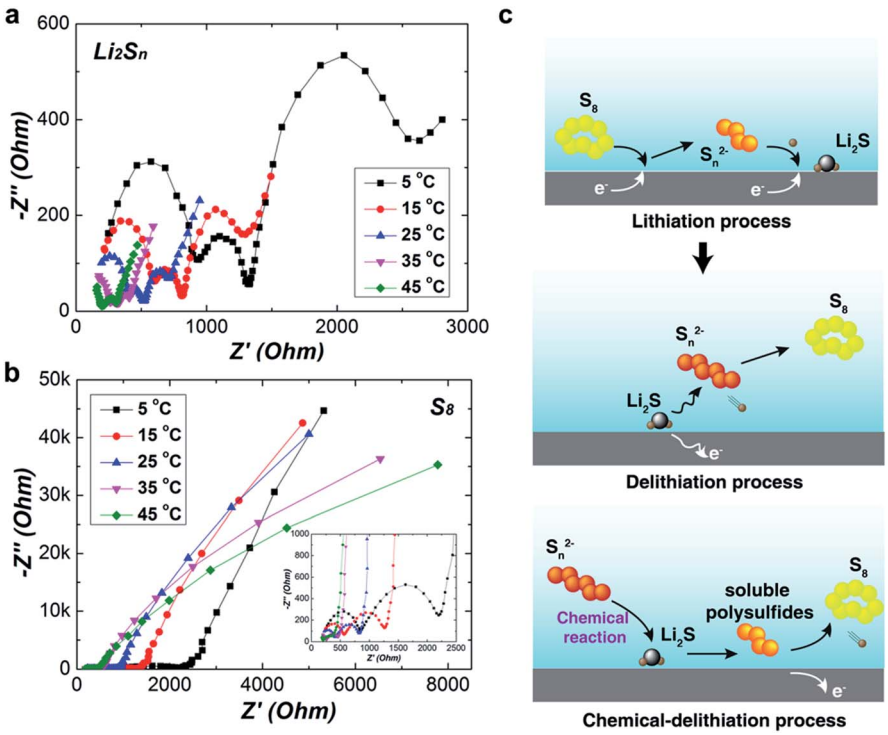

Fig. 4 Nyquist plot of the as-prepared Li–S cell at different temperatures from 5 to 45 °C with (a) Li_2S_n or (b) S_8 catholyte in the frequency region of 1 MHz to 10 mHz. The inset in (b) is an enlarged image of the Nyquist plot in the high frequency region. (c) Illustration of the decomposition behavior of Li_2S through the electrochemical and chemical delithiation process.

bonding environment in Li_2S is more like that in Li_2S_n than in the pure electrolyte,[11] which may facilitate the charge transfer process between Li_2S and Li_2S_n and result in direct chemical reactions between them. As illustrated in Fig. 4c, the catholyte with Li_2S_n is therefore more helpful in oxidizing the solid Li_2S. In consideration of the potential application prospects, the concentration of Li_2S_n can be increased for an improved energy density. The long-chain Li_2S_n ($n > 4$) generally has a high solubility in organic solvents.[7a,12] Therefore, we prepared 1/8 M Li_2S_8 by mixing S_8 and Li_2S powders in a 7 : 8 ratio ($7S_8 + 8Li_2S \rightarrow 8Li_2S_8$) in THF solution containing 1 M $LiClO_4$. The presumed final concentration of Li_2S_8 is 1/8 M, indicating that the S concentration is 1 M. The Li–S cell with the as-prepared Li_2S_8 delivers a stable cycling performance with an average reversible capacity of 600 mA h g^{-1} at 0.1C (Fig. S6, ESI†). The volumetric energy density reaches 13 A h L^{-1} based on the total volume of the catholyte and anolyte.

Conclusions

In summary, we investigated the electrochemical behavior of Li–S batteries with dual-phase electrolytes, in which THF solution containing soluble Li_2S_n or S_8 is employed as the catholyte. In contrast to that with S_8, the cell with Li_2S_n displays a higher specific capacity and rate capability, strongly suggesting generally improved kinetic characteristics. EIS measurements at various temperatures and a combined electrochemical and morphological investigation further prove the improved reaction kinetics of the cell with Li_2S_n, associated with a lower interfacial charge transfer resistance. As a consequence, two insights can be gained: (i) Li_2S_n serving as a supporting electrolyte produces a more efficient charge transfer; and (ii) Li_2S_n acting as a chemical mediator can react with the final discharge product Li_2S through direct chemical reactions, accelerating the reversible decomposition of Li_2S. The work provides insightful information for the design of next- generation liquid flow batteries, considering that a highly concentrated Li_2S_n can potentially be applied in a flow-through mode.

Conflicts of interest

There are no conflicts to declare.

Acknowledgements

The authors acknowledge funding support from the National Natural Science Foundation of China (No. 21603030), the Natural Science Foundation of Shanghai (No. 17ZR1446400), and the Fundamental Research Funds for the Central Universities (No. 2232018D3-02).

Notes and references

1 S. Evers and L. F. Nazar, *Acc. Chem. Res.*, 2012, **46**, 1135–1143.
2 (*a*) A. Manthiram, Y. Fu and Y.-S. Su, *Acc. Chem. Res.*, 2013, **46**, 1125–1134; (*b*) H. Wang, Y. Yang, Y. Liang,

J. T. Robinson, Y. Li, A. Jackson, Y. Cui and H. Dai, *Nano Lett.*, 2011, **11**, 2644–2647; (*c*) J. Zhang, C.-P. Yang, Y.-X. Yin, L.-J. Wan and Y.-G. Guo, *Adv. Mater.*, 2016, **28**, 9539–9544; (*d*) L. Wang, J. Liu, S. Haller, Y. Wang and Y. Xia, *Chem. Commun.*, 2015, **51**, 6996–6999.

3 (*a*) X. Ji, K. T. Lee and L. F. Nazar, *Nat. Mater.*, 2009, **8**, 500–506; (*b*) L. Ji, M. Rao, S. Aloni, L. Wang, E. J. Cairns and Y. Zhang, *Energy Environ. Sci.*, 2011, **4**, 5053–5059; (*c*) L. Wang, Y. Zhao, M. L. Thomas and H. R. Byon, *Adv. Funct. Mater.*, 2014, **24**, 2248–2252; (*d*) M. D. Patel, E. Cha, C. Kang, B. Gwalani and W. Choi, *Carbon*, 2017, **118**, 120–126; (*e*) D. Xiao, Q. Li, H. Zhang, Y. Ma, C. Lu, C. Chen, Y. Liu and S. Yuan, *J. Mater. Chem. A*, 2017, **5**, 24901–24908; (*f*) D. Xiao, C. Lu, C. Chen and S. Yuan, *Energy Storage Materials*, 2018, **10**, 216–222.

4 (*a*) L. Wang and H. R. Byon, *J. Power Sources*, 2013, **236**, 207–214; (*b*) L. Wang, J. Liu, S. Yuan, Y. Wang and Y. Xia, *Energy Environ. Sci.*, 2016, **9**, 224–231; (*c*) S. Chen, F. Dai, M. L. Gordin, Z. Yu, Y. Gao, J. Song and D. Wang, *Angew. Chem., Int. Ed.*, 2016, **55**(13), 4231–4235; (*d*) S. Chen, Z. Yu, M. L. Gordin, R. Yi, J. Song and D. Wang, *ACS Appl. Mater. Interfaces*, 2017, **9**(8), 6959–6966; (*e*) J.-W. Park, K. Ueno, N. Tachikawa, K. Dokko and M. Watanabe, *J. Phys. Chem. C*, 2013, **117**, 20531–20541; (*f*) G. Salitra, E. Markevich, A. Rosenman, Y. Talyosef, D. Aurbach and A. Garsuch, *ChemElectroChem*, 2014, **1**, 1492–1496; (*g*) C. Zu, N. Azimi, Z. Zhang and A. Manthiram, *J. Mater. Chem. A*, 2015, **3**, 14864–14870; (*h*) E. S. Shin, K. Kim, S. H. Oh and W. I. Cho, *Chem. Commun.*, 2013, **49**, 2004–2006; (*i*) M. Cuisinier, P.-E. Cabelguen, B. D. Adams, A. Garsuch, M. Balasubramanianc and L. F. Nazar, *Energy Environ. Sci.*, 2014, **7**, 2697–2705.

5 (*a*) M. J. Lacey, A. Yalamanchili, J. Maibach, C. Tengstedt, K. Edström and D. Brandell, *RSC Adv.*, 2016, **6**, 3632–3641; (*b*) M. Sun, X. Wang, J. Wang, H. Yang, L. Wang and T. Liu, *ACS Appl. Mater. Interfaces*, 2018, **10**, 35175–35183.

6 (*a*) N. Li, Z. Weng, Y. Wang, F. Li, H.-M. Cheng and H. Zhou, *Energy Environ. Sci.*, 2014, **7**, 3307–3312; (*b*) L. Wang, Y. Zhao, M. L. Thomas, A. Dutta and H. R. Byon, *ChemElectroChem*, 2016, **3**, 152–157; (*c*) L. Wang, Y. Wang and Y. Xia, *Energy Environ. Sci.*, 2015, **8**, 1551–1558; (*d*) L. Wang, X. Wang, J. Liu, H. Yang, C. Fu, Y. Xia and T. Liu, *J. Mater. Chem. A*, 2018, **6**, 20737–20745.

7 (*a*) R. D. Rauh, K. M. Abraham, G. F. Pearson, J. K. Surprenant and S. B. Brummer, *J. Electrochem. Soc.*, 1979, **126**(4), 523–527; (*b*) D. Zheng, X. Zhang, C. Li, M. E. Mckinnon, R. G. Sadok, D. Qu, X. Yu, H.-S. Lee, X.-Q. Yang and D. Qu, *J. Electrochem. Soc.*, 2015, **162**, A203–A206.

8 S. I. Tobishima, H. Yamamoto and M. Matsuda, *Electrochim. Acta*, 1997, **42**, 1019–1029.

9 Z. Yang, J. Guo, S. K. Das, Y. Yu, Z. Zhou, H. D. Abruñab and L. A. Archer, *J. Mater. Chem. A*, 2013, **1**, 1433–1440.

10 A. Kawase, S. Shirai, Y. Yamoto, R. Arakawac and T. Takatad, *Phys. Chem. Chem. Phys.*, 2014, **16**, 9344–9350.

11 Y. Yang, G. Zheng, S. Misra, J. Nelson, M. F. Toney and Y. Cui, *J. Am. Chem. Soc.*, 2012, **134**, 15387–15394.

12 Y. Yang, G. Zheng and Y. Cui, *Energy Environ. Sci.*, 2013, **6**, 1552–1558.

